Magnetic Resonance in Medicine 45:838–845 (2001)

Accurate Multislice Gradient Echo T_1 Measurement in the Presence of Non-ideal RF Pulse Shape and RF Field Nonuniformity

Geoffrey J.M. Parker,* Gareth J. Barker, and Paul S. Tofts

A methodology is presented for estimating T_1 using a two-point technique with a standard multislice gradient echo sequence. The method explicitly corrects for the shape of the RF pulse and for spatial variations in transmitted RF field intensity. Including these factors in the calculation of T_1 gives a substantial improvement in accuracy and precision of two-point gradient echo T_1 measurements in the presence of RF nonuniformity and non-ideal pulse profiles. The mean accuracy of the technique was found to be 1.4%. The mean precision was found to be 3.0%. The mean variation along the axis of a head coil was found to be 2.3%. Magn Reson Med 45:838–845, 2001.

Key words: T1; RF nonuniformity; gradient echo; pulse profile

Two-point gradient echo methods provide a convenient in vivo T_1 estimation method and have been applied by numerous workers (e.g., 1–3). They remain a popular method due to their good SNR, low spatial distortion when compared with echo planar techniques, and low power deposition when compared with spin echo techniques. Typically, T_1 information is obtained by comparing the signals obtained from two separate gradient echo image sets acquired with either different repetition times or flip angles (or both). T_1 may then be estimated by employing a theoretical relationship describing the expected effects of T_1 on the signals (assuming a monoexponential longitudinal relaxation). Such two-point techniques are generally insensitive to variations in the receive RF field, but are sensitive to slice profile (especially in the case of multislice 2D) and transmitted B_1 field imperfections. This may cause significant deviations in the calculated T_1 values from the true values (1,3).

To compensate for slice profile effects, it is possible to calibrate the T_1 measurement method, thus giving a result for the effective flip angle through the thickness of the imaging slice (1,3). However, this approach has the drawback of relying on an empirically determined calibration factor, which detracts from the theoretical simplicity of the two-point approach. A more fundamental problem with both the calibration approach and those approaches that attempt to derive T_1 theoretically using the nominal flip angle of the sequence is that they fail in situations where the transmitted RF field is nonuniform. This may occur in coils well known for their nonuniformity, such as surface coils, extremity coils, or breast coils, but also at the edges of generally more uniform volume coils, such as those typically used as head coils and body coils. A possible solution for those wishing to compensate for the effects of slice profile in the presence of such nonuniformity via a calibration method is to determine a 3D calibration field, providing calibration factors at each point within the coil. However, the problems of creating such a field soon become prohibitive, due to the number of T_1 values that must be sampled at each point within the coil to provide an accurate 3D calibration.

Previous workers have looked into the problem of correcting for RF transmission and reception nonuniformity using standard sequences available on clinical scanners. The principal aspect of this problem is determining the transmission and reception field maps within the sensitive region of the coil in question. One frequently used approach is to measure the change in signal observed in a phantom as the RF pulse transmission power is varied. The resulting variation in signal intensity at each point in the coil then provides information about the relative field strength at each point (see, e.g., 4–6). If the reception field of the coil configuration is required, a uniform phantom should ideally be used (6,7) to remove ambiguities due to variation in sample proton density.

An alternative approach to estimating the nonuniformities present in MR images obtained using standard sequences is to utilize postprocessing techniques (see, e.g., 8,9). These techniques, while avoiding the need for special imaging experiments, do not provide estimates of the RF field strengths within the imaging region (they aim to provide the resultant intensity variation), and are unable to distinguish between low spatial frequency anatomical variation and that due to coil nonuniformity. As such, they are poorly suited to correcting for nonuniformities in data acquired for relaxation time measurements.

We present a methodology for estimating T_1 using a two-point gradient echo method, knowledge of the RF pulse shape, and by deriving the coil transmission B_1 distribution. The process does not rely on the calibration of the response of the sequence to different T_1 values, but on the theoretical relationship between flip angle, TR, and T_1, amended to account for slice profile and B_1 variation. We use a gradient echo sequence available as standard on our clinical scanner to show that this technique is accurate and precise and gives uniform results over a large volume within which B_1 is nonuniform.

NMR Research Unit, Department of Clinical Neurology, Institute of Neurology, University College London, Queen Square, London, UK.

Previously presented in an early form at the 7th Annual Meeting of the ISMRM, Philadelphia, 1999 (abstract #2144).

Grant sponsor: Multiple Sclerosis Society of Great Britain and Northern Ireland.

*Correspondence to: Dr. Geoffrey J.M. Parker, NMR Research Unit, Institute of Neurology, University College London, Queen Square, London WCIN 3BG, UK. E-mail: g.parker@ion.ucl.ac.uk

Received 17 February 2000; revised 27 September 2000; accepted 17 November 2000.

Table 1
Gradient Echo Sequence Parameters for T_1 Measurements

Study	θ_{nom}	TE (ms)	TR_1 (ms)	TR_2 (ms)	NEX_1	NEX_2	Matrix	Slices	Slice thickness (mm)	Slice spacing (mm)
1	90°	10	1500	360	2	8	256 × 192	20	5	5
2	45°	11	1500	50	1.5	3	256 × 128	28	5	0

METHODS

All measurements were performed on a General Electric Signa Horizon EchoSpeed 1.5 T scanner running v. 5.7 of the scanner operating system. A standard quadrature birdcage head coil was used for all measurements (General Electric, Milwaukee, WI).

The sequence used to demonstrate the T_1 measurement is a multislice 2D gradient echo (the manufacturer's sequence name is *2dfast).*Two different repetition times (TR_1 and TR_2) were employed, designed to create a predominately proton density-weighted (PDW) dataset and a predominately T_1-weighted (T_1W) dataset, respectively. For simplicity, the flip angle of the slice selective excitation pulse, θ, is kept constant between the two acquisitions.

The exact choice of θ and repetition times for the data acquisitions is not critical for the execution of the T_1 measurement. The principal considerations in the choice are optimization of the SNR of the measurement, assurance of a good dynamic range to the measurement, and an acceptable total measurement time. In this article, we present measurements using two sets of parameters—one being a semiarbitrary set (study 1), and the other being an approximately optimal set for our purposes (study 2) (Table 1). Both measurements as outlined take approximately 19 min for the combined acquisition of both the PDW and T_1W data for whole brain coverage. If a smaller scanning matrix, fewer averages, or shorter TR values were used, this scanning time could be reduced significantly (<1 min). However, our choice of parameters allows us to meet our local requirements for SNR, acquisition time, and resolution. Specifically, the acquisition is to be performed in less than 20 min, have full axial brain coverage using 5 mm slices, have a field of view of 240 × 240 mm, and an in-plane resolution of ≈1 × 1 mm.

Slices within the PDW datasets were acquired in an optimized interleaved mode in two separate subacquisitions, each sampling half the total number of slices. *K*-space lines from alternate slice positions were acquired within a given TR period within each subacquisition. The time between acquisition of *k*-space lines from nearest-but-one slices was automatically maximized within the limit of the 1500 ms TR period by the scanner software. These steps minimized cross-talk between contiguous slice positions due to the extension of the slice profile past the nominal slice thickness.

Each slice from the T_1W dataset was acquired in a sequential mode; the whole of *k*-space for a slice was acquired before moving onto the next slice. The order of slice acquisition was automatically optimized to prevent neighboring slices being sampled close together in time; neighboring slice acquisitions were separated by a number of minutes. This approach enabled the T_1W data also to be acquired without the risk of slice crosstalk. The effects of steady-state transverse magnetization were counteracted using RF spoiling and assumed to be negligible. Possible magnetization transfer effects due to off-resonance irradiation during the interleaved acquisition used for the PDW acquisition were assumed to be insignificant.

All data acquisitions (including phantom data) were made with reference to the same landmark position on the head coil. This ensured that positional references were maintained for compensation for the effects of RF field nonuniformity. All scanner gains and the RF transmitter frequency were manually kept constant between the PDW and T_1W data acquisitions to ensure identical data sampling and scaling conditions for the T_1 calculation steps.

Pulse Profile

We define the nominal flip angle, θ_{nom}, of a pulse as the flip angle requested by the user on the scanner interface. The automatic prescan procedure of the GE Signa scanner attempts to set the center of the slice profile to this nominal value within a slice at the center of the imaging volume (10); we assume this process is reproducible and accurate in all measurements (that any errors in this process are small). For any non-top-hat profile, all other flip angles in the slice profile will not equal θ_{nom}.

The first step in our methodology for T_1 calculation requires knowledge of the time-varying amplitude profile of the pulse used in the sequence for slice selection and spin excitation. The time-domain pulse profile was obtained using the "ESE" software package provided by the scanner manufacturer (General Electric) for the design and analysis of RF pulses. This profile represents the exact waveform fed into the RF amplifiers driving the imaging coil. A Bloch simulation of the resultant response of the magnetization vector across a 5 mm imaging slice immediately after the application was obtained (again using the ESE software) over a range of nominal flip angles at 10° intervals. T_1 was set to 1000 ms and T_2 to 100 ms for the simulation to give conditions similar to those seen in vivo at 1.5 T. However, dependence on T_1 and T_2 is negligible during the time period covered by the RF pulse, meaning the simulation is insensitive to the exact choice of these parameters. Plots for a selection of flip angles and a plot of the time domain pulse are shown in Fig. 1. These show the components of the rotating frame transverse magnetization that may be expected after the application of the RF pulse. The actual flip angle, θ(ζ) at a point ζ along a line perpendicular to the slice plane is determined by:

$$\tan^{-1}\theta(\zeta) = \frac{\sqrt{M_x(\zeta)^2 + M_y(\zeta)^2}}{M_z(\zeta)}, \qquad [1]$$

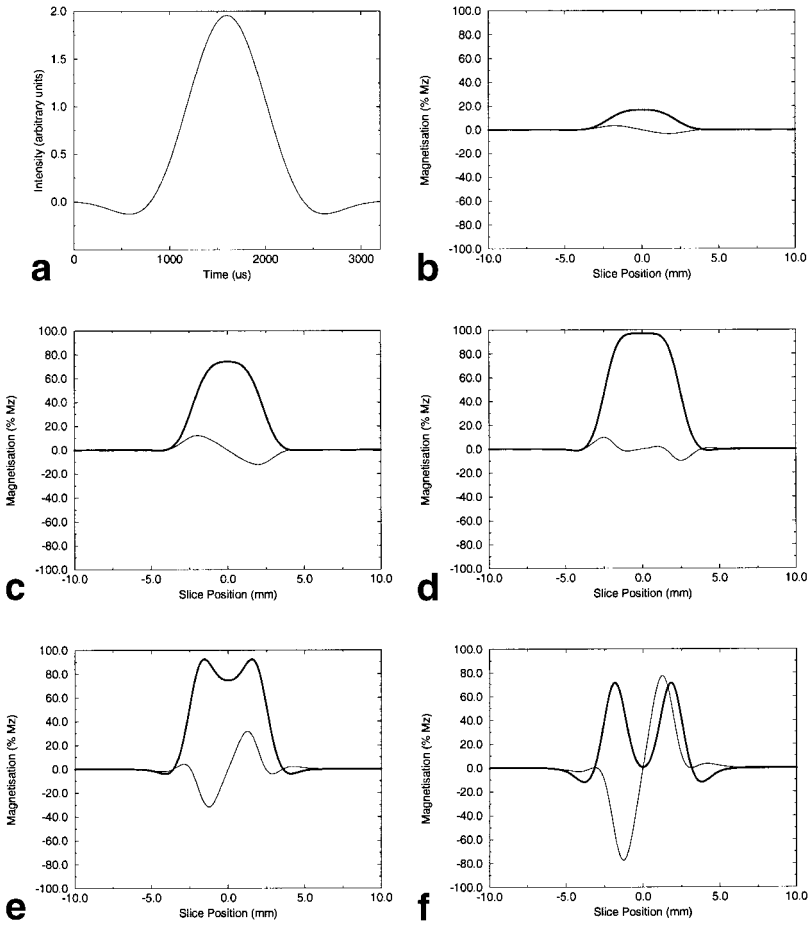

FIG. 1. **a:** Time domain profile of the excitation pulse. **b–f:** Transverse magnetization components as a function of position within the slice (nominal slice width 5 mm) at increasing θ_{nom}. θ_{nom} equals: (**b**) 10°, (**c**) 50°, (**d**) 90°, (**e**) 130°, (**f**) 180°. Bold line represents M_x; thin line represents M_y, as a percentage of the equilibrium longitudinal magnetization, M_z.

where $M_x(\zeta)$, $M_y(\zeta)$, $M_z(\zeta)$ are the *x, y, z* components of the magnetization vector as viewed in the rotating frame at point ζ.

Theoretical Signal Intensity Calculation With Pulse Profile

The signal from a spoiled gradient echo imaging sequence when the (ideal) flip angle is θ, is given by (11) (assuming T_2^* effects are negligible (that TE $\ll T_2^*$)):

$$S = \frac{S_0\left(1 - \exp\left(-\frac{\mathrm{TR}}{\mathrm{T1}}\right)\right)\sin\theta}{1 - \cos\theta\exp\left(-\frac{\mathrm{TR}}{\mathrm{T1}}\right)}, \qquad [2]$$

where S_0 is a constant describing the scanner gain (including coil reception strength) and proton density (it is the signal obtained when $\theta = 90°$ with a long TR). This equation holds for an entire imaging voxel only for a perfect slice profile, with uniform θ across the slice. However, as may be appreciated from Fig. 1 and Eq. [1], in cases where the flip angle varies substantially through the imaging slice, there is not a single value of θ that describes the behavior across the whole slice width and Eq. [2] is not appropriate.

To overcome the problem of a variable flip angle across the slice, the function shown in Eq. [2] may be integrated across the slice profile, providing an estimate of the true total signal in response to the pulse. However, as can be seen in Fig. 1, there is a significant contribution to the magnetization vector from both $M_x(\zeta)$ and $M_y(\zeta)$, meaning that the phase of the transverse magnetization, $\phi(\zeta)$, during the repeated TR periods must be incorporated. This is accomplished by separately integrating the $M_x(\zeta)$ and $M_y(\zeta)$ components of the transverse magnetization and substituting the magnetization components for signal intensity in Eq. [2]:

$$M_x = A\int_{slice}\left\{\frac{\left(1 - \exp\left(-\frac{\mathrm{TR}}{\mathrm{T1}}\right)\right)\sin(\theta(\zeta))\cos(\phi(\zeta))}{1 - \cos(\theta(\zeta))\exp\left(-\frac{\mathrm{TR}}{\mathrm{T1}}\right)}\right\}d\zeta, \qquad [3]$$

$$M_y = A\int_{slice}\left\{\frac{\left(1 - \exp\left(-\frac{\mathrm{TR}}{\mathrm{T1}}\right)\right)\sin(\theta(\zeta))\sin(\phi(\zeta))}{1 - \cos(\theta(\zeta))\exp\left(-\frac{\mathrm{TR}}{\mathrm{T1}}\right)}\right\}d\zeta, \qquad [4]$$

where A is a constant of proportionality. By converting to a discrete summation over the slice profile and again exploiting the direct proportionality between signal and transverse magnetization, we have:

$$S_x = A' \sum_{n=1}^{N} \left\{ \frac{\left(1 - \exp\left(-\frac{\mathrm{TR}}{\mathrm{T1}}\right)\right)\sin(\theta(n))\cos(\phi(n))}{1 - \cos(\theta(n))\exp\left(-\frac{\mathrm{TR}}{\mathrm{T1}}\right)} \right\} \quad [5]$$

$$S_y = A' \sum_{n=1}^{N} \left\{ \frac{\left(1 - \exp\left(-\frac{\mathrm{TR}}{\mathrm{T1}}\right)\right)\sin(\theta(n))\sin(\phi(n))}{1 - \cos(\theta(n))\exp\left(-\frac{\mathrm{TR}}{\mathrm{T1}}\right)} \right\}, \quad [6]$$

where S_x and S_y are the x and y components of the signal (the *real* and *imaginary* components); N is the number of discrete samples, n, along the slice profile sampled at equally spaced intervals; and A' is a constant of proportionality. For this study we use $N = 800$. The total signal is then:

$$S = \sqrt{S_x^2 + S_y^2}. \quad [7]$$

Equations [4] and [6] equal zero for the pulse used in this work (the y component of the magnetization is antisymmetric, as may be seen by inspection of Fig. 1). However, this is not necessarily the case for all RF pulses, and the y component of the magnetization and signal is presented here to aid understanding of the process.

The values of $\theta(n)$ scale with the nominal flip angle, θ_{nom}, with a maximum flip angle within the profile, θ_{max}, at the center of the profile. Due to the presence of RF nonuniformity within the imaging volume, θ_{max} is not in general equal to θ_{nom}.

Coil B_1 Distribution

The coil B_1 distribution was determined by acquiring contiguous images throughout the coil using the sequence introduced above with a long TR and variable nominal flip angle. A bottle of approximately 20 cm diameter and 30 cm in length was filled with vegetable oil to provide a uniform nonconducting phantom which fills the head coil well without any conductivity or standing wave-associated RF nonuniformities (12–15). The same sequence was used for the B_1 measurement as for the T_1 measurement. The T_1 of vegetable oil is approximately 200 ms at room temperature (7); TR was set to 3000ms to reduce T_1 dependence to a negligible level. 65 slices were acquired with a 5 mm slice thickness and no slice gap and a field of view of 280 × 280 mm.

Datasets were acquired with a range of nominal flip angle:

$$\theta_{nom} \in \{45°, 55°, 65°, 75°, 85°, 90°, 95°, 105°, 115°, 125°, 135°, 145°, 155°, 165°, 175°, 180°\}. \quad [8]$$

The dependence of the signal intensity, S, on the flip angle, θ, at any point in the coil, $\mathbf{r}$, is governed by Eqs. [5]–[7] as long as the flip angle at the center of the profile ($\theta_{max}(\mathbf{r})$) is known. We introduce $\delta(\mathbf{r})$ is a factor describing the transmission B_1 field strength at point $\mathbf{r}$, relative to the field strength required to produce θ_{nom} (in a slice at the center of the coil, as discussed above). $\theta_{max}(\mathbf{r})$ is then defined by:

$$\theta_{max}(\mathbf{r}) = \delta(\mathbf{r})\theta_{nom}. \quad [9]$$

As we are using a phantom with uniform proton density, T_1 and T_2 for all $\mathbf{r}$, we may assume that $A'(\mathbf{r})$ (Eqs. [5],[6]) is proportional to the reception RF field at point $\mathbf{r}$ in the coil. We assume that changes in $\delta(\mathbf{r})$ are slow relative to the slice thickness; that a single value of $\delta(\mathbf{r})$ may be defined for each voxel.

To determine $\delta(\mathbf{r})$ at each point within the imaging volume, a lookup table was created. The table contains values of θ_{max} and the resultant expected signal, $S(\mathbf{r})$, generated using Eqs. [5]–[7], over a range of ($0° < \theta_{max} < 180°$), at a resolution of 0.1°. The acquisition sequence was repeated for each θ_{nom} (Eq. [8]). The resultant $S(\mathbf{r})$ for each θ_{nom} varies according to the values of $\theta_{max}(\mathbf{r})$. This variation at point $\mathbf{r}$ is then matched to values of θ_{max} in the lookup table, to provide $\theta_{max}(\mathbf{r})$, and, via Eq. [9], $\delta(\mathbf{r})$, the transmit RF field strength relative to the field strength at the coil center.

We assume that the RF distribution determined in the oil phantom is a good approximation to that produced when the head coil is loaded with a head (16–18).

Calculation of T_1

To obtain T_1 values, a second lookup table is created based on Eqs. [5–7]. This lookup table relates the ratio ($R(T_1)$) of the T_1W signal intensity accounting for pulse profile (S_{T1W}) and the PDW signal intensity accounting for slice profile (S_{PDW}) to T_1:

$$R(T_1) = \frac{S_{\mathrm{T1W}}}{S_{\mathrm{PDW}}} = \frac{\sqrt{S_{\mathrm{T1W}_x}^2 + S_{\mathrm{T1W}_y}^2}}{\sqrt{S_{\mathrm{PDW}_x}^2 + S_{\mathrm{PDW}_y}^2}}, \quad [10]$$

where S_{T1W_x} and S_{T1W_y} are the x and y components creating the T_1W signal and S_{PDW_x} and S_{PDW_y} are the x and y components creating the PDW signal. S_{PDW} and S_{T1W} are determined using TR_1 and TR_2, respectively, in Eqs. [5], [6].

T_1 may be estimated for any B_1 value within the bounds of this lookup table using Eq. [9] to define θ_{max}. A match is made for θ_{max} and $R(T_1)$ to give T_1. The process of taking the ratio removes any dependence of the method upon the strength of the receive RF field and the gain settings of the scanner, as A' (Eqs. [5],[6]) is canceled. Any influence of transverse magnetization relaxation on signal intensity will be the same for both S_{T1W} and S_{PDW}, and is also canceled out at this step, even if our initial assumption that transverse relaxation effects are negligible does not hold (Eq. [2]).

Accuracy and Uniformity of T_1 Measurements

The accuracy of the T_1 measurement technique was determined using agarose gel samples (Eurospin Test Object 5; Diagnostic Sonar, Livingston, UK). The T_1 values of these samples were themselves validated independently of the

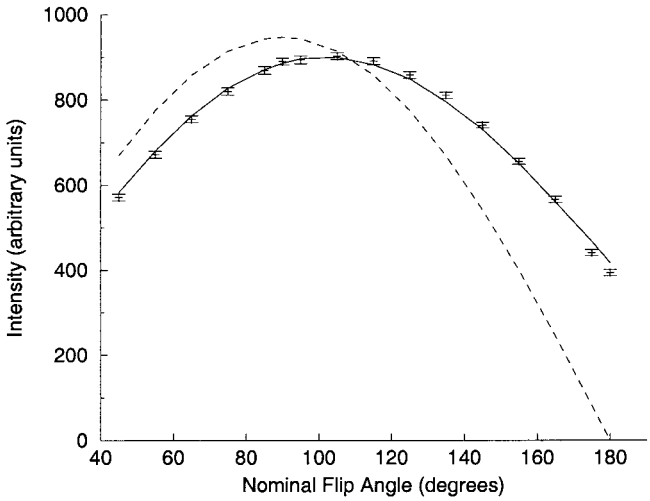

FIG. 2. Variation in signal intensity with θ_{nom} (TR $\gg T_1$). Solid line represents curve fitted using the lookup table method. For reference, the dotted line shows best fit of Eq. [2] (estimated response, not taking into account slice profile effects).

proposed measurement technique, using a single slice long TR inversion recovery spin echo sequence (TR = 10,000 ms; TE = 14 ms; field of view = 200 × 200 mm; slice thickness = 20 mm; image matrix = 256 × 128; NEX = 1). The inversion times (TI) used were: 50, 75, 100, 125, 150, 200, 300, 400, 500, 700, 1000, 2000, 3000 ms. The values measured using this sequence, and the gradient echo sequence described previously, both with and without taking into account pulse profile and RF nonuniformity, were compared.

The variation of calculated T_1 within the head coil measured using the two-point gradient echo method after correction for slice profile and RF nonuniformity was assessed by measuring the T_1 value for each gel along the axis of a head coil over a distance of approximately 17 cm. The mean and standard deviation of T_1 over this range was calculated, from which the coefficient of variation, COV, was determined.

RESULTS

Figure 2 shows how the signal at the center of the coil varies with nominal flip angle. The point at which maximum signal is obtained is approximately 105°, indicative of the non-sinusoidal behavior of the signal–flip angle relationship (an ideal best-fit sine curve, as obtained under ideal top-hat slice profile conditions, is shown for reference). The solid curve closely matching the data points is that obtained when the effects of slice profile on the expected signal are included in the fitting process. As discussed above, the effects of B_1 nonuniformity are assumed to be negligible at the center of the coil; that $\theta_{nom} = \theta_{max}$.

Figure 3 shows the relative transmit RF field within the transmit-receive head coil as measured using the procedure outlined in Methods. As expected, the slices far from the coil center display the largest degree of inhomogeneity and average difference to the values at the center of the coil. This is particularly evident toward the inferior end of the coil (negative slice positions).

From the multipoint inversion recovery T_1 measurement of the T_1 samples it was evident that the gel sample T_1 values had shortened during their time in our laboratory (approximately 5 years) by an average of approximately 15% per sample (data not shown), implying a lack of long-term stability in these reference gels under local storage conditions. Our measurements using the multipoint IR sequence were therefore taken as our gold standard ("true") T_1 values. Figure 4 shows measured values at the center of the coil using the two-point gradient echo sequence with and without accounting for pulse profile and RF intensity. A large improvement is visible after accounting for these factors. For Fig. 4 the true T_1 values were measured at 20.5°C; study 1 at 21°C; study 2 at 23°C. The mean accuracy and mean precision of the study 1 protocol were determined from five measurements taken over a period of weeks (temperature range 20–22°C). The mean accuracy (defined as the mean value of $|T1_{\mathrm{meas}} - T1_{\mathrm{true}}| \times 100/T1_{\mathrm{true}}$ for each sample, averaged over all samples) was 1.4% (range between samples = 0.21–2.82%). The precision (defined as the percentage standard deviation of each sample measurement, averaged over all samples) was 3.0% (range between samples =

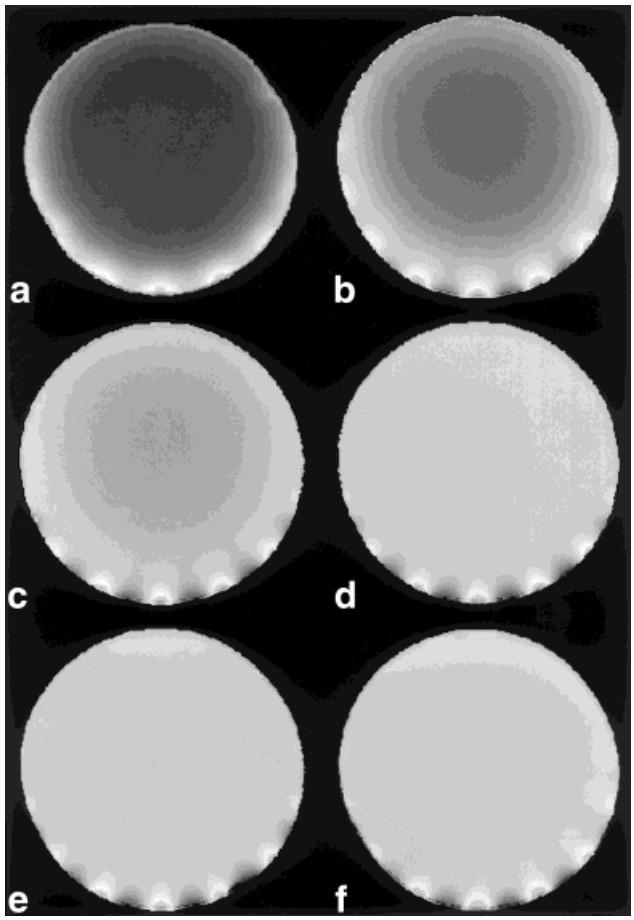

FIG. 3. Transmit RF field in oil bottle in head coil at five different axial slice positions, windowed to show nonuniformity: (**a**) −110 mm; (**b**) −90 mm; (**c**) −50 mm; (**d**) 0 mm; (**e**) +50 mm; (**f**) +90 mm.

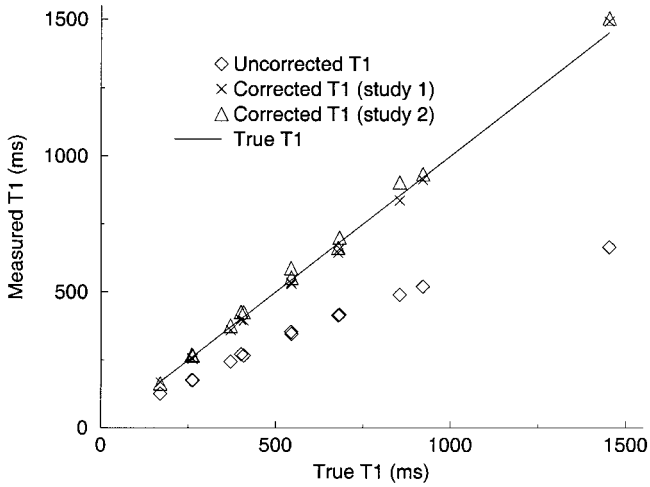

FIG. 4. T_1 measurements, corrected and uncorrected for slice profile, performed in an axial slice located at the center of the head coil.

1.8–4.8%). Figure 5 shows how apparent T_1 values vary along the *z* axis of the head coil, both with (Fig. 5b) and without (Fig. 5a) accounting for pulse profile and RF uniformity. After correction, the mean COV along the *z* axis over all T_1 samples is 2.3% (COV range between samples = 1.9–3.4%). The effect of correcting for slice profile is to shift the T_1 values closer to the gold standard. The effect of correcting for the coil nonuniformity is apparent from the elimination of a position dependency.

Figure 6 shows T_1 maps calculated using the study 2 protocol within the brain of a normal volunteer. As can be seen, the method provides high resolution, high SNR T_1 measurements, with a high degree of volume coverage. No artifactual fall-off in the values of T_1 with coil position is apparent. Figure 7 shows T_1 histograms obtained from all tissues in the dataset from which the images in Fig. 6 were drawn. A shift in the peak positions for white matter, gray matter, and scalp is apparent after profile correction. The effect of nonuniformity correction alone is smaller (as we are looking at the entire head, much of which is in a relatively uniform region of the coil (Fig. 3)), but still significant.

DISCUSSION AND CONCLUSIONS

We have shown that using knowledge of the sequence pulse profile and a measured coil B_1 field it is possible to obtain uniform, accurate, two-point T_1 measurements, even in the presence of imperfect pulse profiles and B_1 fields that are not ideal. We found that the theoretical relationship between flip angle, TR, and T_1 for a gradient echo two-point T_1 measurement holds only when these factors are taken into account explicitly. This approach therefore avoids the need for calibration of two-point gradient echo T_1 measurements against T_1 standards (3). As a standard sequence is used, there is no requirement for programming specialist T_1 measurement techniques. We believe that this fact makes our approach attractive when compared with other RF-insensitive T_1 measurement techniques, such as inversion recovery or saturation recovery centric-ordered turboFLASH, Look-Locker, or TOMROP approaches (11,19–24).

Recent work by Brookes et al. (25) has followed a parallel path to the work presented here. However, our T_1 measurements have a much better agreement with the true T_1 values in T_1 phantoms than their published results. This may be due to a number of methodological differences. They do not include any correction for B_1 field inhomogeneity, and therefore experience severe difficulty outside the most uniform regions of imaging coils. Their determination of the time-varying pulse profile relied on monitoring the output RF channel signal using an oscilloscope, rather than exploiting the data files used to generate the pulse. This is a matter of convenience, and may be the only way of obtaining the pulse profile if the scanner manufacturer does not make it available. These authors came to the conclusion that gradient echo methods (especially 2D multislice methods) should be held in suspicion

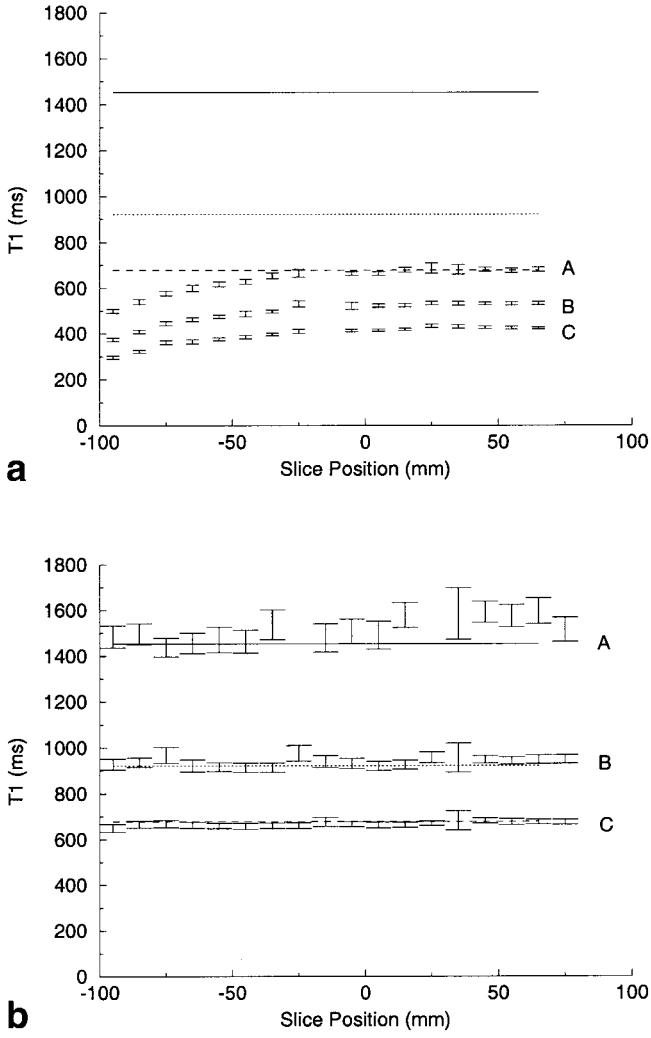

FIG. 5. **a:** T_1 values estimated using the nominal flip angle (θ_{nom}) and not correcting for field nonuniformity. **b:** T_1 values obtained after accounting for the pulse profile and the measured coil transmit RF field. Solid lines: true T_1 sample A; dotted lines: true T_1 sample B; dashed lines: true T_1 sample C. Error bars represent standard deviation of T_1 within each region of interest.

when used for T_1 measurements. However, our results suggest that by carefully accounting for all significant sources of error, robust T_1 measurements are possible.

The method presented here relies on the accurate determination of the flip angle, θ_{nom}, at the center of the coil. The flip angle calibration process relied on for this work exists on General Electric scanners only; other manufacturers use alternative methods. If an equivalent definition of θ_{nom} is not available on other scanners, the possibility of introducing the method described (10) could be considered as a manual alternative to the default manufacturer's method. Alternatively, the relationship between the method described in Ref. 10 and the local method could be established as a one-off calibration step.

The process of determining the strength of the transmitted RF field differs from those described previously (see, e.g., Refs. 4–6), as these did not correct for the effects of the slice profile. Doing so allows the non-sinusoidal behavior of the flip angle–signal strength relationship to be modeled successfully (Fig. 2). Our method for determining the transmit RF field inhomogeneity assumes that the RF distribution measured in a large oil phantom closely approximates that produced when the coil is loaded by a head. This assumption appears reasonable at 1.5 T; at higher field strengths this is not so (16–18).

Although for the purposes of correcting T_1 measurements we have focused on the measurement of the transmitted RF field, this technique also provides information concerning the reception fields of the coil configuration used for the imaging process (as long as a uniform oil phantom is used). This allows the two effects to be determined separately. Thus, we expect this technique to be of use when an imaging coil is used in receive-only mode (for example, a phased array), with a separate coil being used for transmission. In these circumstances the independent transmission and reception fields can be assessed.

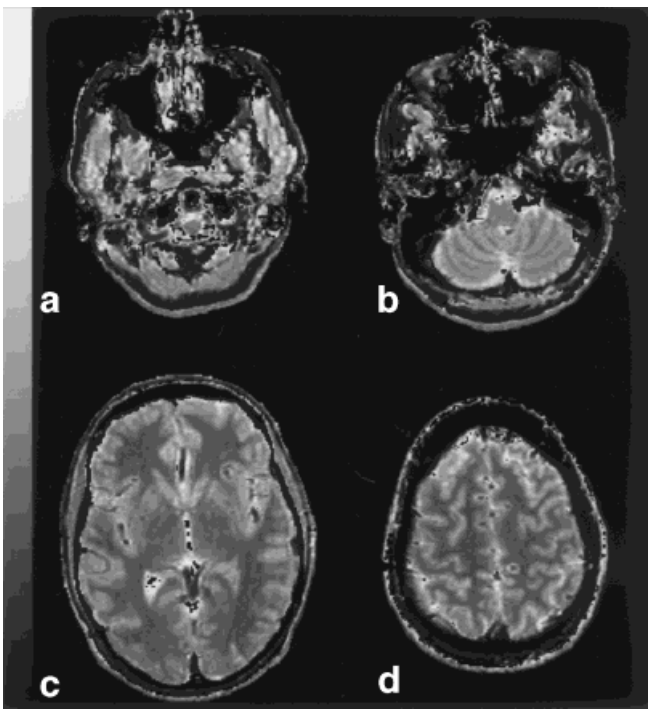

FIG. 6. T_1 maps in the brain of a normal volunteer. Slice positions (relative to landmark at naison): (**a**) −62.5 mm; (**b**) −37.5 mm; (**c**) 7.5 mm; (**d**) 57.5 mm. Gray scale range 0 ms $< T_1 <$ 2500 ms.

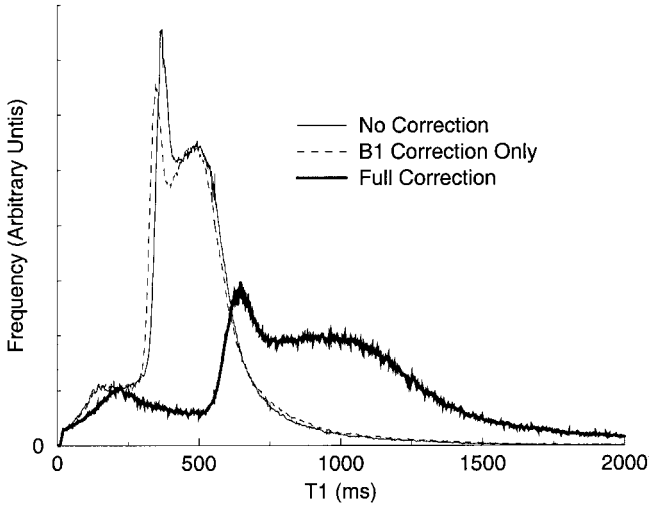

FIG. 7. T_1 histograms obtained from the head of a normal volunteer, smoothed with a moving average window of 20 ms. The results for no correction for B_1 nonuniformity or pulse profile, correction for B_1 nonuniformity only, and for full correction are shown. In each of the histograms the left-hand peak is caused by scalp; the middle peak by white matter; the broad peak on the right by gray matter.

This technique allows T_1 to be measured with confidence in coils exhibiting RF inhomogeneity and with standard sequences having non-ideal pulse profiles. A possible application is the measurement of pathological T_1 values in the central nervous system, with particular emphasis on the measurement of T_1 values in multiple sclerosis in the brain and spinal cord. Clinically important regions, such as the brain stem (Fig. 6a), often fall in nonuniform regions of imaging coils (26), leading to difficulties in determining relaxation times in such regions.

ACKNOWLEDGMENTS

We thank Martin King and Andrew Lowe for assistance and Peter Jezzard for useful comments on the relationship between RF uniformity in phantoms and in vivo.

REFERENCES

1. Brookes JA, Redpath TW, Gilbert FJ, Needham G, Murray AD. Measurement of spin-lattice relaxation times with FLASH for dynamic MRI of the breast. Br J Radiol 1996;69:206–214.
2. Fram EV, Herfkens RJ, Johnson GA. Rapid calculation of T1 using variable flip angle gradient refocused imaging. Magn Reson Imag 1987; 5:201–208.
3. Parker GJM, Suckling J, Tanner SF, Padhani AR, Revell PB, Husband JE, Leach MO. Probing tumor microvascularity by measurement, analysis and display of contrast agent kinetics. J Magn Reson Imag 1997;7:564–574.
4. Insko EK, Bolinger L. Mapping of the radiofrequency field. J Magn Reson Ser A 1993;103:82–85.
5. Wicks DAG, Barker GJ, Tofts PS. Correction of intensity nonuniformity in MR images of any orientation. Magn Reson Imag 1993;11:183–196.
6. Barker GJ, Simmons A, Arridge SR, Tofts PS. A simple method for investigating the effects of non-uniformity of radiofrequency transmission and radiofrequency reception in MRI. Br J Radiol 1998;71:59–67.

7. Tofts PS, Barker GJ, Dean TL, Gallagher AP, Gregory AP, Clarke RN. A low dielectric constant customized phantom design to measure RF coil nonuniformity. Magn Reson Imag 1997;15:69–75.
8. Held K, Kops ER, Krause BJ, Wells WM, Kikinis R, Müller-Gärtner H-W. Markov random field segmentation of MR images. IEEE Trans Med Imag 1997;16:878–886.
9. Sled JG, Zijdenbos AP, Evans AC. A nonparametric method for automatic correction of intensity nonuniformity in MRI data. IEEE Trans Med Imag 1998;17:87–97.
10. King KF, Licato PE, Slayman BE, Crawford CR. Fast flip angle calibration. In: Proc 3rd Annual Meeting ISMRM, Nice, France, 1995. p 699.
11. Haase A. Snapshot FLASH MRI. Applications to T1, T2, and chemical shift imaging. Magn Reson Med 1990;13:77–89.
12. Parker GJM, Rowland IJ, Collins DJ, Leach MO. Investigation of factors affecting uniformity in test objects and the advantages of using polydimethylsiloxane (PDMS). In: Proc 2nd Annual Meeting ISMRM, Berkeley, 1994. p 203.
13. Simmons A, Tofts PS, Barker GJ, Arridge SR. Sources of nonuniformity in spin echo images at 1.5 T. Magn Reson Med 1994;32:121–128.
14. Tofts PS. Standing waves in uniform water phantoms. J Magn Reson Ser B 1994;104:143–147.
15. Tofts PS, Barker GJ, Simmons A, MacManus DG, Thorpe J, Gass A, Miller DH. Correction of nonuniformity in images of the spine and optic nerve from fixed receive-only surface coils at 1.5 T. J Comput Assist Tomogr 1994;18:997–1003.
16. Collins CM, Li S, Smith MB. SAR and B1 field distributions in a heterogeneous human head model within a birdcage coil. Magn Reson Med 1998;40:847–856.
17. Collins CM, Smith MB. Calculated B1 homogeneity, SNR, and SAR vs. frequency for the head in an idealized quadrature birdcage coil. In: Proc 7th Annual Meeting ISMRM, Philadelphia, 1999. p 417.
18. Allecci M, Collins CM, Smith MB, Jezzard P. B1 field plots for a 3 Tesla birdcage coil: concordance of experimental and theoretical results. In: Proc 8th Annual Meeting ISMRM, Denver, 2000. p 1391.
19. Bluml S, Schad LR, Stepanow B, Lorenz WJ. Spin-lattice relaxation time measurement by means of a turboFLASH technique. Magn Reson Med 1993;30:289–295.
20. Parker GJM, Baustert I, Tanner SF, Leach MO. Improving image quality and T1 measurements using saturation recovery turboFLASH with an approximate k-space normalization filter. Magn Reson Imag 2000;18:157–168.
21. Look DO, Locker DR. Time saving in measurement of NMR and EPR relaxation times. Rev Sci Instrum 1970;41:250–251.
22. Kay I, Henkelman RM. Practical implementation and optimization of one-shot T1 imaging. Magn Reson Med 1991;22:414–424.
23. Brix G, Schad LR, Deimling M, Lorenz W. Fast and precise T1 imaging using a TOMROP sequence. Magn Reson Imag 1990;8:351–356.
24. Gowland P, Mansfield P. Accurate measurement of T1 in vivo in less than 3 seconds using echo-planar imaging. Magn Reson Med 1993;30:351–354.
25. Brookes JA, Redpath TW, Gilbert FJ, Murray AD, Staff RT. Accuracy of T1 measurement in dynamic contrast-enhanced breast MRI using two- and three-dimensional variable flip angle fast low-angle shot. J Magn Reson Imag 1999;9:163–171.
26. Stevenson VL, Parker GJM, Birnie K, Tofts P, Barker GJ, Miller DH, Thompson AJ. Variations in T1 and T2 relaxation times of normal appearing white matter and lesions in multiple sclerosis. J Neurol Sci 2000;178:81–87.